PASJ: Publ. Astron. Soc. Japan , 1–??,

On Black Hole Mass Estimation from X-ray Spectra of Ultraluminous X-ray Sources

Kiki VIERDAYANTI[1,*], Ken-ya WATARAI[2,3,†], and Shin MINESHIGE[1,*]
[1] *Yukawa Institute for Theoretical Physics, Kyoto University, Sakyo-ku, Kyoto 606-8502*
[2] *Astronomical Institute, Osaka Kyoiku University, Asahigaoka, Kashiwara, Osaka 582-8582*
[3] *Kanazawa University Fuzoku High School, Heiwa-machi, Kanazawa, Ishikawa 921-8105*
kiki@yukawa.kyoto-u.ac.jp

(Received 2007 December 6; accepted 2008 February 13)

Abstract

We propose a methodology to derive a black-hole mass for super-critical accretion flow. Here, we use the extended disk blackbody (extended DBB) model, a fitting model in which the effective temperature profile obeys the relation $T_{\rm eff} \propto r^{-p}$, with r being the disk radius and p being treated as a fitting parameter. We first numerically calculate the theoretical flow structure and its spectra for a given black-hole mass, M, and accretion rate, $\dot{M}$. Through fitting to the theoretical spectra by the extended DBB model, we can estimate the black-hole mass, $M_{\rm x}$, assuming that the innermost disk radius is $r_{\rm in} = 3r_{\rm g}(\propto M_{\rm x})$, where $r_{\rm g}$ is the Schwarzschild radius. We find, however, that the estimated mass deviates from that adopted in the spectral calculations, M, even for low-$\dot{M}$ cases. We also find that the deviations can be eliminated by introducing a new correction for the innermost radius. Using this correction, we calculate mass correction factors, $M/M_{\rm x}$, in the super-critical regimes for some sets of M and $\dot{M}$, finding that a mass correction factor ranges between $M/M_{\rm x} \sim 1.2$ – 1.6. The higher is $\dot{M}$, the larger does the mass correction factor tend to be. Since the correction is relatively small, we can safely conclude that the black holes in ULXs which Vierdayanti et al. (2006, PASJ, 58, 915) analyzed are stellar-mass black holes with the mass being $< 100 M_\odot$.

Key words: accretion, accretion disks — black hole physics — X-rays: stars

1. Introduction

The most intriguing question regarding the ultraluminous X-ray sources (ULXs) at present would be how massive is the black hole in each ULX.

Known to be very bright extragalactic X-ray sources ($L_{\rm x} \sim 10^{39-41}{\rm ergs}^{-1}$), brighter than the ever-known Galactic X-ray sources, ULXs are good candidate to prove the existence of the hypothetical new class of black holes, the intermediate mass black holes (IMBHs), whose masses range over 10^2 – 10^4 $M_\odot$ (e.g. Colbert & Mushotzky 1999; Makishima et al. 2000). If we simply assume $L_{\rm x} \leq L_{\rm E}$, where $L_{\rm E}$ is the Eddington luminosity, $M \geq 10^3 M_\odot$ for $L_{\rm x} \sim 10^{41}$ erg s^{-1}. This provides strong support to the IMBH hypothesis.

The success in fitting the spectra of several ULXs with a multicolor disk blackbody (DBB) and a power-law (PL) model further supports the idea of IMBHs for the ULXs, since the cool inner disk temperatures and the large innermost radii, obtained through model fitting, suggest a black hole mass within the IMBH range (Miller et al. 2003,2004; Cropper et al. 2004, Roberts et al. 2005). Moreover, the explanation behind the IMBH notion for ULXs is based on the standard accretion disk model (Shakura & Sunyaev 1973), a well-established model for high-energy release mechanism through gas accretion flows around a compact object.

On the other hand, some attempts have been made to challenge the IMBH interpretation of ULXs (King et al. 2001). Several models have been proposed to allow stellar-mass black holes to power ULXs. In fact, such attempts are very reasonable since the existence of stellar-mass black holes is well founded while IMBH formation has not been well understood (e.g. Madhusudhan et al. 2006).

Amongst several models proposed, a model of super-critical accretion flow onto a stellar-mass black hole has been quite favorable recently (e.g., Watarai et al. 2001; Okajima et al. 2006; Vierdayanti et al. 2006; Tsunoda et al. 2006). One attractive model supporting a super-critical accretion flow onto a stellar-mass black hole is the slim disk model (Watarai et al. 2000; Kawaguchi 2003, Ebisawa et al. 2003; Okajima et al. 2006) introduced in the late 1980s by the Warsaw and the Kyoto groups (Abramowicz et al. 1988, 1989, see Kato et al. 2008 for a review). Its application to some Galactic black holes was investigated by Watarai et al. (2000) in their attempts to explain the nature of some bright X-ray source binaries. Later on, Watarai et al. (2001) also proposed the slim disk model for ULXs.

* Present Affiliation: Department of Astronomy, Kyoto University, Sakyo-ku, Kyoto 606-8502
† Research Fellow of the Japan Society for the Promotion of Science

The black-hole mass mentioned above was estimated from an X-ray spectral fitting in which the innermost radius, $r_{\rm in}$, was assumed to coincide with that of the last stable circular orbit, $r_{\rm ms}$ ($=3r_{\rm g}$ for a non-rotating black hole, where $r_{\rm g}$ [$\equiv 2GM/c^2$] is the Schwarzschild radius). This assumption has been proven to be good for the cases of Galactic black hole binaries (e.g., Makishima et al. 1986; Tanaka & Shibazaki 1996; Ebisawa 1999; Dotani et al. 1997).

However, numerical calculations have shown that as mass accretion rate increases, the flow inside $3r_{\rm g}$ might produce significant emission (Watarai et al. 2000). The heat generated near $3r_{\rm g}$ is trapped by the inward material flows, and is emitted inside $3r_{\rm g}$. Some amount of the trapped radiation going closer to the black hole is swallowed. Therefore, since the situation is more complicated in high mass accretion rate systems, we cannot simply relate the innermost radius from the fitting with the last stable circular orbit. Indeed, Watarai and Mineshige (2003a) have stressed that the observed value of the inner edge of the disk is more like a radiation edge, outside of which substantial emission is produced. In this work, we investigated the assumption $r_{\rm in}=3r_{\rm g}$ for the super-critical accretion flows around a non-rotating black hole and calculate corrections to make more accurate black-hole mass estimations.

The plan of this paper is as follows:

We describe the disk structure and spectrum calculations in the first two subsections in section 2, and the fitting model, together with the conventional method to derive black hole mass from the fitting in the remaining subsection.

In section 3, we present our fitting analysis and results, while focusing on some sets of parameters.

Section 4 is devoted to a discussion, and finally section 5 concludes the paper.

2. Methodology

To avoid confusion, we will first describe the overall picture of our methodology which is also summarized in table 1. The detail steps in the fitting are explained in another section (section 3).

The main steps of our methodology are as follows: We first calculate the disk structure for various values of black-hole mass, M, and the mass-accretion rate, $\dot{M}$ (subsection 2.1). Next, we use the outputs from the disk structure calculation to obtain the spectra (subsection 2.2). We follow the calculation by Watarai et al. (2005) for both steps. We then fit those spectra with the extended DBB model and derive the black hole mass, $M_{\rm x}$ from value of $r_{\rm in}$ obtained from the fitting (subsection 2.3). That is, we assume $r_{\rm in}=3r_{\rm g}$ as that of the DBB model. Finally, we obtain the correction factor, $M/M_{\rm x}$, the ratio of the actual black hole mass to the derived black hole mass (subsection 3.2).

2.1. Disk Structure Calculation

The standard accretion-disk model has been very successful in describing optically thick flow structure as long as the mass accretion rate of the systems in question is less than the critical mass-accretion rate [1], $\dot{M}\le\dot{M}_{\rm crit}\equiv L_{\rm E}/c^2$.

It is possible, however, that the mass-accretion rate of a system exceeds the critical mass-accretion rate in disk accretion because of anisotropic radiation field (Ohsuga et al. 2005). A disk in which its accretion rate exceeds the critical value is called a super-critical accretion disk.

In this section we describe the calculation of the structure of such a disk (e.g., Watarai et al. 2000, 2005; see reviews by Kato et al. 2008). The equations are written by using cylindrical coordinates (r,φ,z). A non-rotating black hole is assumed as the central object and a pseudo-Newtonian potential (Paczyński & Wiita 1980) is adopted to model the general relativistic effects in the gravitational field of the black hole,

$$\psi=-\frac{GM}{R-r_{\rm g}}, \tag{1}$$

where $R=\sqrt{r^2+z^2}$.

The pressure and density are related to each other by polytropic relation (Hōshi 1977), $p\propto\rho^{1+\frac{1}{N}}$, in the vertical direction, where N is the polytropic index. The vertically integrated density, Σ, and pressure, Π, are then

$$\Sigma\equiv\int_{-H}^{H}\rho dz=\int_{-H}^{H}\rho_0\left(1-\frac{z^2}{H^2}\right)^N dz=2\rho_0 I_N H, \tag{2}$$

$$\Pi\equiv\int_{-H}^{H}p dz=\int_{-H}^{H}p\left(1-\frac{z^2}{H^2}\right)^{N+1} dz=2p_0 I_{N+1} H, \tag{3}$$

where

$$I_N=\frac{(2^N N!)^2}{(2N+1)!}, \tag{4}$$

and H is the scale height.

Assuming hydrostatic balance in the vertical direction, we have

$$\Omega_{\rm K}^2 H^2=2(N+1)\frac{p_0}{\rho_0}, \tag{5}$$

where $\Omega_{\rm K}$ is the Keplerian angular velocity of the disk rotation in the pseudo-Newtonian potential, which is defined by

$$\Omega_{\rm K}=\left(\frac{\partial\psi}{r\partial r}\right)^{1/2}\Bigg|_{z=0}=\frac{r}{r-r_g}\left(\frac{GM}{r^3}\right)^{1/2}. \tag{6}$$

Note that in terms of Π and Σ, the hydrostatic balance in the vertical direction can be written as

$$\Omega_{\rm K}^2 H^2=(2N+3)\frac{\Pi}{\Sigma}. \tag{7}$$

Regarding the polytropic index, we set $N=3$ for the whole disk calculation.

[1] Some papers use $\dot{M}_{\rm crit}\equiv L_{\rm E}/(\eta c^2)$ with η, the energy conversion efficiency, being a constant. However, this may cause confusion since η is not constant in the slim disk model.

Table 1. The overall picture of our methodology.

Step	Calculation	Input	Output	Section
1	Disk structure	M, $\dot{M}$	$T_{\rm eff}(r)$, $H(r)$, $v_r(r)$, $v_\varphi(r)$	2.1
2	Spectrum	$T_{\rm eff}(r)$, $H(r)$, $v_r(r)$, $v_\varphi(r)$	S_ν	2.2
3	Fitting	S_ν	$T_{\rm in}$, $r_{\rm in}$, p	2.3
4	Correction factor	$r_{\rm in}$, M	$M/M_{\rm x}$	3.2

The other basic equations are obtained by integration in the vertical direction under the assumption that the radial velocity, v_r, and the specific angular momentum, ℓ ($= r v_\varphi = r^2\Omega$), do not depend on the vertical coordinate.

The continuity equation gives

$$-2\pi r \Sigma v_r = \dot{M} = \text{constant}, \tag{8}$$

where $\dot{M}$ is the mass accretion rate.

The radial component of the momentum equation can be written as

$$v_r \frac{dv_r}{dr} + \frac{1}{\Sigma}\frac{d\Pi}{dr} = \frac{\ell^2 - \ell_{\rm K}^2}{r^3} - \frac{\Pi}{\Sigma}\frac{d\ln\Omega_{\rm K}}{dr}, \tag{9}$$

where $\ell_{\rm K}$ is the Keplerian angular momentum, defined by $\ell_{\rm K} = r^2\Omega_{\rm K}$. The last term of the above equation, $\frac{\Pi}{\Sigma}\frac{d\ln\Omega_{\rm K}}{dr}$, is a correction term resulting from the fact that the radial component of the gravitational force changes with height (Matsumoto et al. 1984).

The angular-momentum balance is obtained from the φ-component of momentum equation, and can be written as

$$\dot{M}(\ell - \ell_{\rm in}) = -2\pi r^2 T_{r\varphi}, \tag{10}$$

where $\ell_{\rm in}$ is an integration constant, which represents the specific angular momentum finally swallowed by the black hole, and $T_{r\varphi}$ is the vertical integration of $t_{r\varphi}$, that is

$$T_{r\varphi} \equiv \int_{-H}^{H} t_{r\varphi} dz = -\alpha\Pi, \tag{11}$$

with $t_{r\varphi} = -\alpha p$ as in the standard Shakura-Sunyaev prescription.

The energy equation can be written as

$$Q_{\rm adv}^- = Q_{\rm vis}^+ - Q_{\rm rad}^-, \tag{12}$$

where $Q_{\rm adv}^-$ is the advective cooling, defined by

$$Q_{\rm adv}^- = \int_{-H}^{H} q_{\rm adv}^- dz = \frac{9}{8} v_r \Sigma T_{\rm c} \frac{ds}{dr}, \tag{13}$$

where s is the specific entropy on the equatorial plane. The viscous energy generation rate is given by

$$Q_{\rm vis}^+ = \int_{-H}^{H} q_{\rm vis}^+ dz = r T_{r\varphi} \frac{d\Omega}{dr}, \tag{14}$$

while the radiative cooling rate is given by

$$Q_{\rm rad}^- = \int_{-H}^{H} q_{\rm rad}^- dz = 2F, \tag{15}$$

where F is the radiative flux per unit surface area on the disk surface, given by

$$F = \frac{8acT_{\rm c}^4}{3\tau}, \tag{16}$$

where a is radiative constant, $T_{\rm c}$ is the temperature on the equatorial plane, and τ is given by

$$\tau = \bar{\kappa}\Sigma = (\kappa_{\rm es} + \kappa_{\rm ff})\Sigma. \tag{17}$$

The equation of state is given by

$$\Pi = \Pi_{\rm gas} + \Pi_{\rm rad} = \frac{k_{\rm B}}{\bar{\mu} m_{\rm H}} \frac{I_4}{I_3} \Sigma T_{\rm c} + \Pi_{\rm rad}, \tag{18}$$

where $\Pi_{\rm rad}$ is defined by

$$\Pi_{\rm rad} \equiv \int_{-H}^{H} \frac{1}{3} a T_{\rm c}^4 \left(1 - \frac{z^2}{H^2}\right)^4 dz. \tag{19}$$

We first specify the values of M, α, $\dot{M}$, and an initial guess of $\ell_{\rm in}$. The outer boundary conditions are imposed at $r = 1\times10^4 r_{\rm g}$, where all physical quantities are taken as those of the standard disk. The inner calculation boundary is taken at $r \sim 2.0 r_{\rm g}$. Note that it is important to solve the equations, even inside the marginally stable last circular orbit at $3r_{\rm g}$, since substantial amount of matter still exists there. In fact, the emission from this region makes a rather important contribution when $\dot{M} \geq 100\dot{M}_{\rm crit}$. Also note that it is possible to calculate the disk structure inside $2r_{\rm g}$, but in this region the disk in fact becomes optically thin and thus the blackbody assumption made in calculating the spectrum may no longer be valid. Further, the contribution from the innermost part at $r < 2r_{\rm g}$ is small because of a photon redshift. Thus, we left this region for our future studies.

The solution should satisfy the regularity condition at the transonic radius located between (2 – 3) $r_{\rm g}$ and the free boundary conditions at the inner edge. The basic equations are first radially integrated for an a priori given $\ell_{\rm in}$. When $\ell_{\rm in}$ is larger (or smaller) than the correct value, the radial velocity vanishes (diverges) before $r_{\rm g}$. Iteration of $\ell_{\rm in}$ is therefore needed to find an appropriate value for which a transonic solution is obtained. In other words, the value of $\ell_{\rm in}$ is determined uniquely by the transonic condition.

2.2. Spectrum Calculation

In calculating the spectrum, we apply a calculation method proposed by Watarai et al. (2005). They adopted the 'Ray-Tracing method' (Luminet 1979; Fukue & Yokoyama 1988) in calculating the spectra of a disk around a Schwarzschild black hole. Before reaching the observer, a photon emitted from some point on the disk travels along the null geodesics. In the Schwarzschild space-time, the photon's trajectory is determined by

$$\frac{d^2}{d\chi^2}\left(\frac{1}{r}\right)+\frac{1}{r}=\frac{3r_{\rm g}}{2r^2}, \tag{20}$$

where r is the distance from the center (black hole), and χ is the angle measured from the direction of the observer (see reviews by Kato et al. 2008). The trajectories will then satisfy the following differential equation:

$$\left[\frac{d}{d\chi}\left(\frac{1}{r}\right)\right]^2+\frac{1}{r^2}\left(1-\frac{r_{\rm g}}{r}\right)=\frac{1}{b^2}, \tag{21}$$

where b is the impact parameter.

The light ray is calculated from an observer's coordinate to the surface of the disk by the 'Runge-Kutta-Gill Method' and the scale-height is defined as the disk surface of the last scattering. The numerical integration is stopped when the ray arrives at the surface of the disk, and the final arrival point is interpolated from the calculated data of the disk model. The obtained quantities, such as temperature, velocity field, and redshift on the disk surface, are transformed to the observer's values, which are used to calculate the observed spectrum.

The observed spectra were calculated by using the Lorentz invariant relation,

$$I_{\nu_{\rm obs}}=\left(\frac{\nu_{\rm obs}}{\nu_{\rm em}}\right)^3 I_{\nu_{\rm em}}\approx\frac{1}{(1+z)^3}B_{\nu_{\rm em}}(T_{\rm eff}), \tag{22}$$

where $I_{\nu_{\rm em}}$ and $\nu_{\rm em}$ are the intensity and frequency in the disk co-moving frame, respectively. Some simplifications are also made here, that the blackbody radiation, $B_\nu(T_{\rm eff})$, is assumed in order to calculate the spectra, and the temperature on the disk surface is adopted as the effective temperature. The thermal Comptonization process, which may become important in the innermost region, is approximated by introducing a spectral hardening factor, κ. We set $\kappa=1.7$ throughout the calculation (see discussion in subsection 4.2). The local flux is calculated by using a diluted blackbody approximation,

$$F_\nu^{\rm db}=\frac{1}{\kappa^4}\pi B_\nu(\kappa T_{\rm eff}). \tag{23}$$

The redshift factor, $(1+z)$, which consists of a gravitational redshift part and the Doppler parts, is given by,

$$1+z=\frac{E_{\rm em}}{E_{\rm obs}}=L^{-1}\gamma D^{-1}, \tag{24}$$

where L, γ, and D are the lapse functions representing the gravitational redshift, Lorentz factor, and Doppler factor, respectively (Kato et al. 2008).

According to Watarai et al. (2005), the inclination-angle dependence of the accretion disk spectrum is composed of the following three factors:

1. The projection effect, which is the change of the effective area with the change of the inclination angle.
2. The effect of Doppler beaming towards the observer's direction, which causes asymmetry in the flux distribution with respect to the rotation axis.
3. The self-occultation effect (Fukue 2000), that is, the central part of the disk is obscured by the cooler outer part of the disk. This effect is significant for high-inclination systems.

Note that self-irradiation (Cunningham 1975) was not considered in the present study.

The spectrum calculation done by Watarai et al. (2005) was not intended for calculating the spectrum over a large area of the disk. We made a simple modification to make the calculation for larger disk area possible with reasonable calculation time. This is necessary since the spectra of the high mass-accretion rate disks extend into the soft X-ray region (Szuszkiewicz et al. 1996). To do so, we divided the disk by following $\sqrt{r}$ pattern. By doing so, we can keep the detail of the innermost part without losing those of the outermost part too much.

2.3. Fitting Model

In this subsection we switch to a description of the fitting model and the conventional method to derive the black hole mass.

2.3.1. Extended disk blackbody model

The fitting model that we describe in this section, and is the main tool used in this work, is the extended disk blackbody (extended DBB) model. This X-ray spectral fitting model was originally proposed by Mineshige et al. (1994) to investigate whether the temperature gradient found from the observations of Nova Muscae 1991 could deviate from the canonical value of the standard disk, 0.75 ($T_{\rm eff}\propto r^{-3/4}$).

The name 'extended DBB' is chosen, because it is a natural extension of the DBB model [2]. It becomes a generalization and an extension of the DBB model, since the temperature gradient is now treated as one of the fitting parameters. The temperature profile, hence, becomes,

$$T_{\rm eff}=T_{\rm in}\left(\frac{r}{r_{\rm in}}\right)^{-p}, \tag{25}$$

where $T_{\rm in}$ and $r_{\rm in}$ have the same interpretation as those in the DBB model.

By using self-similar solutions, Watarai and Fukue (1999) found that the temperature distribution of the slim disk is somewhat flatter than that of the standard disk, that is $T_{\rm eff}\propto r^{-1/2}$ (see also Wang & Zhou 1999). Therefore, the temperature profile of the standard disk is proportional to $r^{-3/4}$, while for the case of slim disk, $r^{-1/2}$.

Generally speaking, hence, by using the extended DBB model, r^{-p}, for the fitting, we can distinguish the case where the standard disk is more plausible than the slim disk, and vice versa, from the spectrum profile.

2.3.2. Conventional methodology to derive black-hole mass

When we obtain a good fit to the observed spectra by the DBB model, we can easily estimate the black-hole mass and the Eddington ratio, $L/L_{\rm E}$ (with L and $L_{\rm E}$ being disk luminosity and the Eddington luminosity, respectively), based on the standard disk theory.

[2] In some papers it is called the 'p-free'model, but we do not use it, since this is a confusing terminology.

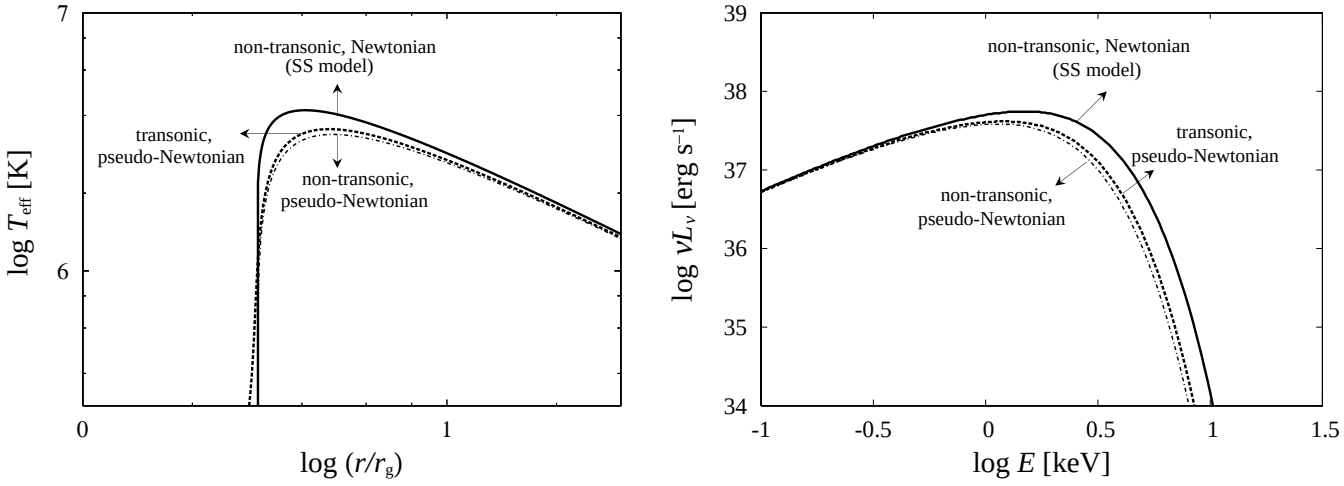

Fig. 1. Comparison between the standard disk model (Shakura and Sunyaev 1973; analytical Newtonian non-transonic solution) in solid lines and the numerical model (pseudo-Newtonian, transonic solution) at low $\dot{m}$ ($\dot{m}=1$), in dashed lines. Left panel: effective temperature profiles. Right panel: Spectra. We also plot analytical pseudo-Newtonian non-transonic solution in thin dot-dashed lines.

The basic methodology is summarized in Makishima et al. (2000).

We write the bolometric luminosity of an optically thick accretion disk as

$$L_{\rm bol} = 2\pi D^2 f_{\rm bol} (\cos i)^{-1}, \tag{26}$$

with $f_{\rm bol}$ being the bolometric flux, i being the inclination of the disk ($i=0$ corresponds to face-on geometry) and D is the distance. This $L_{\rm bol}$ is related to the maximum disk color temperature, $T_{\rm in}$, and the innermost disk radius, $r_{\rm in}$, as

$$L_{\rm bol} = 4\pi (r_{\rm in}/\xi)^2 \sigma (T_{\rm in}/\kappa)^4, \tag{27}$$

where $\kappa \sim 1.7$ (Shimura & Takahara 1995) is the ratio of the color temperature to the effective temperature, or spectral hardening factor, and $\xi = 0.412$ is correction factor reflecting the fact that $T_{\rm in}$ occurs at somewhat larger than $r_{\rm in}$.

Hence, the innermost disk radius is

$$r_{\rm in} = \xi \kappa^2 \sqrt{\frac{L_{\rm bol}}{4\pi\sigma T_{\rm in}^4}}. \tag{28}$$

We may identify $r_{\rm in}$ with the radius of the last stable Keplerian orbit. Thus, we may in general write

$$r_{\rm in} = 3\beta r_{\rm g} = 8.86\beta (\frac{M}{M_\odot}) \text{ km} \quad \text{with} \quad \frac{1}{6} < \beta \leq 1 \tag{29}$$

by which we can determine the black hole mass. Note that β depends on the black hole spin and $\beta = 1/6$ for an extremely rotating Kerr black hole, and $\beta = 1$ for a Schwarzschild black hole. In the present study, we focus on the cases of the Schwarzschild black hole ($\beta = 1$).

2.3.3. Problem with the Conventional Methodology

The extended DBB model is a phenomenological model which was proposed to investigate a possible deviation of the temperature gradient from 0.75, the value predicted by the theory of the standard disk. It turned out that this model can also be useful to discriminate the slim disks from the standard disks, as explained in the previous part.

However, physical interpretation of the fitting results by using the extended DBB model is far from being clear, unlike in the case of DBB model. We need a methodology to make a physical interpretation of the extended DBB model in the light of the super-critical accretion-disk theory.

In the case of ULXs, Vierdayanti et al. (2006), for example, have tried to make a physical interpretation of the fitting results from the extended DBB fitting model. They adopted a method that is widely used for the DBB fitting model which corresponds to the standard disk theory to derive black hole masses from the fitting results. The fitting shows the tendency that the observational data of the analyzed ULXs are more likely to be fitted with the slim disk model. We realized that the adoption of the conventional method used for the DBB model is not fully appropriate, since the spectral shapes of the slim disk is different from those of the standard disk. Therefore, the adoption of the conventional method is inadequate for estimating the black hole mass. In addition, a number of relativistic effects as well as self-occultation effect certainly affect the spectra, and thus the fitting results. The implication of such relativistic cases are not obvious, and have been poorly investigated so far. In conclusion, some correction should be introduced to permit this adoption. To be precise, in the following section we will try to find a mass correction factor, defined as $m/m_{\rm x}$, where m ($\equiv M/M_\odot$) and $m_{\rm x}$ ($\equiv M_{\rm x}/M_\odot$) are the original black-hole mass and the black-hole mass obtained from the fitting, respectively.

Table 2. The fitting steps (see text for definition of $\xi^{\rm trans}$, and $M/M_{\rm x}$).

Step	Fitted Model	$\dot{m}$-value	Corrections	Section
0	Shakura-Sunyaev model	1,10	$\xi = 0.412$	3.1
1	Numerical transonic model	1,10,32,100,320,1000	$\xi^{\rm trans} = 0.353$, $M/M_{\rm x}$ (for high-$\dot{M}$)	3.1 and 3.2

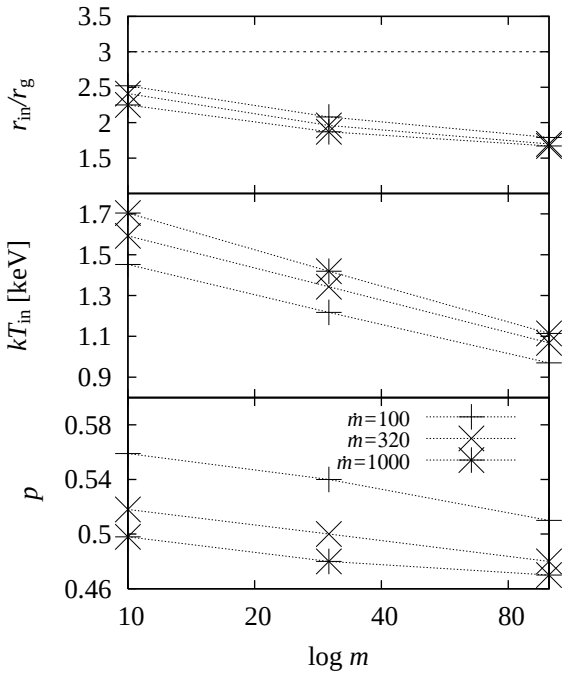

Fig. 2. Fitting results: p (bottom panel), $kT_{\rm in}$ (middle panel), and $r_{\rm in}/r_{\rm g}$ (top panel) with $\dot{m} = 100$, 320, and 1000 and $i = 0$ for various m.

3. Fitting Analysis and Results

We fit the theoretical spectra of the slim disk (Watarai et al. 2005) with the extended DBB model. In the theoretical spectrum calculation, there are three parameters that should be determined in the disk structure calculation, whose results are used to calculate the spectra. They are, the black-hole mass, $m(\equiv M/M_{\odot})$, the mass-accretion rate, $\dot{m}(\equiv \dot{M}c^2/L_{\rm E})$, and the viscosity parameter, α. Regarding the viscosity parameter, in this study we only focus on $\alpha = 0.01$. Another parameter is needed in the spectrum calculation, that is the inclination angle of the disk or the viewing angle of the observer. On the other hand, there are three fitting parameters in the extended DBB model, $T_{\rm in}$, $r_{\rm in}$, and p. We divide our fitting procedure into two important steps, which are summarized in table 2.

To relate $r_{\rm in}$ with the radius of the inner edge of the disk, we need a correction, ξ. However, we found numerically that the ξ-value does not coincide with the analytically expected one, $\xi = 0.412$. Hence, we firstly fit two disk models, analytical standard disk model and numerical disk model for low $\dot{m}$-case, with the extended DBB model to find the basic corrections, which will be explained in the following subsection. The details are given in subsection 3.1

Secondly, after we found the basic corrections we applied them to the high $\dot{m}$-case. This step is described in subsection 3.2.

3.1. Basic Corrections

As a first step of our fitting, we elucidate some basic corrections that were set aside in some previous studies. We call them basic corrections, since they emerged from the disk structure calculation before we calculated the spectra.

In the fitting with the extended DBB model, which is just an extension of the DBB model, we expect the same results for both analytical standard disk model and numerical disk model for the case of moderately low $\dot{m}$, $\dot{m} \leq 1$. This is because theoretically, the disk should behave like a standard disk when $\dot{m}$ is moderately low. On the other hand, it should deviate from that of the standard disk when $\dot{m}$ is moderately high, since the assumptions made for the standard disk case will break down.

Interestingly, our fitting results show some discrepancies even for a moderately small $\dot{m}$ case. We studied some previous works and come to a conclusion that a possible source of discrepancies is q small deviation of the numerical disk model from that of the standard disk. (cf. Ebisawa et al. 1991; Kubota et al. 1998: Kubota 2001). In order to prove it, we compared the numerical transonic flow model in a pseudo-Newtonian potential with the analytical Shakura and Sunyaev (SS) model (in which the transonic nature of the flow is not considered) in a Newtonian potential.

The left panel of figure 1 shows the effective temperature profiles of both models. The solid lines represent the analytical result of Shakura-Sunyaev model, while the dashed lines represent that of the transonic model for $m = 10$ and $\dot{m} = 1$. We can see that even at low $\dot{m}$, a discrepancy exists, especially in the innermost region, where the transonic solution plays its role and the effect of different potential forms is more significant. We then calculate the spectra of both models by using the spectrum calculation code of Watarai et al. (2005). However, here and only when it is stated, we neglect the relativistic Doppler and light bending effects for simplicity. The results are shown in the right panel of figure 1. In addition, we also plot analytical pseudo-Newtonian non-transonic solution as a comparison (thin dot-dashed lines in figure 1). As shown in figure 1, the effect of the difference in the choice of potential form is more prominent compared to the effect of transonic/non-transonic solution.

The discrepancy in the temperature profiles shows that we need a correction factor in addition to κ for the inner temperature. In order to find the required correction

Table 3. Fitting results with the extended DBB model for $\alpha = 0.01$ and $i = 0$. The unit for $kT_{\rm in}$ is keV and energy range for fitting is 0.3 – 10 keV. The luminosity is calculated for all energy range (not only 0.3 – 10 keV).

m	$\dot{m}$	p	$kT_{\rm in}$	$r_{\rm in}/r_{\rm g}$	$\kappa^{\rm trans}$	$\xi^{\rm trans}$
10	1	0.637	0.53	2.96	1/1.19	0.353
10	10	0.634	0.96	2.79	1/1.15	0.353
30	1	0.639	0.40	2.97	1/1.18	0.351
30	10	0.621	0.74	2.72	1/1.14	0.351

factor, we calculate the spectrum of those two disk structure models without considering any spectral hardening effect, i.e., we set $\kappa = 1$ and compare the values of $T_{\rm in}$. We found that $T_{\rm in}$ of the numerical model is by a factor of ~ 1.2 lower than that of the standard disk. Thus, in fitting the numerical disk model with the extended DBB fitting model, the inner temperature correction $T_{\rm in}^{\rm SS}/T_{\rm in} = 1.2$ is required in addition to κ, where $T_{\rm in}^{\rm SS}$ in the inner temperature of the Shakura-Sunyaev model. Therefore, it is necessary to define $\kappa^{\rm real} \equiv \kappa^{\rm trans}\kappa$, as a real correction for the inner temperature, where $\kappa^{\rm trans} = 1/1.2$ and $\kappa \sim 1.7$ for Compton scattering.

We found that the innermost radius, $r_{\rm in}$, also deviates from that of the standard disk. Note that in calculating $r_{\rm in}$, we have used the bolometric luminosity, and thus the luminosity does not depend on the fitting energy range. We decided to handle this deviation separately from that of the temperature. The reason is to keep the black-hole mass estimation method simple. That is, we can simply obtain $r_{\rm in}$ from the $T_{\rm in}$ (without correcting it first), and just add the correction at the end of the procedure, that is after we obtain the estimated black hole mass. The correction for $T_{\rm in}$ becomes important when we want to estimate the mass accretion rate which is not the focus of our present study.

By using the uncorrected $T_{\rm in}$ in the fitting, the deviation in the innermost radius can be eliminated by changing the correction factor, ξ, introduced earlier (see subsubsection 2.3.2). In our present study, we found that the new value of ξ, $\xi^{\rm trans} = 0.353$ is more appropriate instead of $\xi = 0.412$ which is commonly used (cf. Gierliński et al. 1999). We summarize the fitting results in table 3.

We notice that the p-value obtained by the fitting is not close to $p = 0.75$ but significantly lower, $p < 0.64$. This reflects a bit flatter temperature profile of the transonic solution (see figure 1)

3.2. Fitting Results for High $\dot{m}$-case

Now, for applying to the ULXs, we examine the high $\dot{m}$-case. Here, we apply the correction that we found in low $\dot{m}$-case to the high $\dot{m}$-case. That is, we use $\xi^{\rm trans} = 0.353$. Note that in addition to κ we also found necessary correction for the inner temperature, which is $\kappa^{\rm trans} = 1/1.2$, and thus the real correction for the inner temperature is $\kappa^{\rm real} = \kappa/1.2$. However, as we decided to treat this correction separately, the most important basic correction for our fitting methodology is the new value of ξ, which is $\xi^{\rm trans} = 0.353$, while still using $\kappa \sim 1.7$ instead of $\kappa^{\rm real} = \kappa^{\rm trans}\kappa$ for the fitting. The detailed results of the fitting are summarized in table 4 and 5.

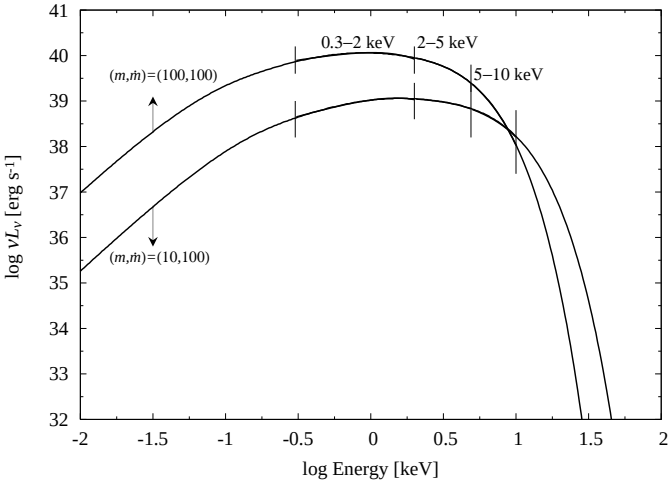

Fig. 3. Fitting range sample

3.2.1. m-dependence

Firstly, let us see the fitting results for different black hole masses. We calculated the spectra of the slim disk for $m = 10$, 30, and 100, fixed $\dot{m}$ at 100, and considered the face-on case only, $i = 0$ in this subsection. Let us focus on the inner temperature, $kT_{\rm in}$, and p (figure 2).

We see that the inner temperature, $kT_{\rm in}$, decreases as the mass increases. This is natural, since the more massive is the black hole the lower is the temperature, as $T_{\rm in} \propto M^{-1/4}$. Interestingly, the value of p behaves in the same way, which is not obvious. It is important to note that p is determined by the slope in the lower energy (soft X-ray) region (Watarai et al. 2000), that is the middle part of the spectrum. The disk spectrum is shifted to the lower energy region as the mass increases (see Fig. 3). In other words, a fixed fitting energy range corresponds to a different part of the spectrum for different black hole mass (see figure 3 for illustration). This is the reason why p depends on the black-hole mass.

We found that the higher is the black hole mass, the smaller is the p-value (see table 4). Note that recent X-ray fitting of some ULX spectra with the extended DBB model also showed that $p \sim 0.5$. This is natural if we jump to conclusion that those ULXs have high black-hole masses based on our finding above. However, a small p can also be obtained even by a stellar-mass black hole with a high mass-accretion rate, which is discussed more in the next subsection. The important thing is that the dependence of p on black-hole mass that we found here is natural, since we restrict the fitting energy range.

Now, let us see the behavior of the inner radius obtained from the fitting. We found that the inner radius also depends on the black-hole mass; a larger black-hole mass has a smaller $r_{\rm in}/r_{\rm g}$. In the fitting, the innermost radius is mainly determined by the high-energy part of the spectrum (inner region of the disk). The dependence of the

inner radius on the black-hole mass shows that the shapes of the spectrum from the inner part of the disk change with the black-hole mass. In other words, the spectrum of the inner part of the disk of a massive black hole is not a simple scale up of that of the stellar-mass black hole (cf. Abramowicz et al. 1988). However, the difference is small and becomes less prominent in the lower energy part (outer part of the disk).

3.2.2. $\dot{m}$-dependence

Now, let us see the fitting results for various mass accretion rate, $\dot{m}$ (table 4). The most interesting result is the luminosity. In the theory of a slim disk, the luminosity at first increases as the mass-accretion rate increases. However, above a certain value, the radiation efficiency decreases as the advection effect becomes dominant, and the luminosity increases not at the same rate as the mass-accretion rate (Jaroszyński et al. 1980). In other word, the luminosity is saturated above a certain mass-accretion rate value.

We found that the luminosity rapidly increases as we increase $\dot{m}$ from 32 to 100. As we further increase $\dot{m}$ up to 1000, slower increase in luminosity is realized (figure 4). In other words, our results are in good agreement with the theory, and thus justifies our methodology. Note that the fitting results of the luminosity for different black hole masses coincide in figure 4.

As we briefly mentioned above, p decreases as $\dot{m}$ increases which is also in good agreement with theoretical prediction. Since as $\dot{m}$ increases the heat is trapped in the flow of matter and thus the advective, horizontal heat flux becomes important (Abramowicz et al. 1988). In other words, the effective temperature gradient becomes flatter as $\dot{m}$ increases, and thus p decreases. Although higher black hole mass gives lower p-value, it is important to remember that a higher black-hole mass also gives a lower $T_{\rm in}$. Therefore, it is more likely that a lower mass black hole with higher mass accretion rate can explain high temperature, low p-value ULXs.

3.2.3. i-dependence

Lastly, we would like to show the behavior of the spectra for various inclination angles. We mentioned earlier when we described the spectrum model of Watarai et al. (2005) that the spectral shape of their model strongly depends on the inclination angle as the mass accretion rate increases. Let us now see the fitting results for various inclination angles. Here, we fixed $\dot{m} = 100$, and $m = 10$, 30, and 100 (table 5). The inner temperature of the disk at first tends to increase as the inclination angle increases, but a sudden drop is realized at an inclination angle above 50° (figure 5). The slight increase in $kT_{\rm in}$ at low inclination angles is basically caused by the Doppler boosting, while a sudden drop above 50° is caused by the self-obscuration effect. Note that we obtained very similar trend even for different black hole masses. In this study, we focus on the case for inclination angle below 50° to explain ULXs with high inner temperature, as suggested by Watarai et al. (2005).

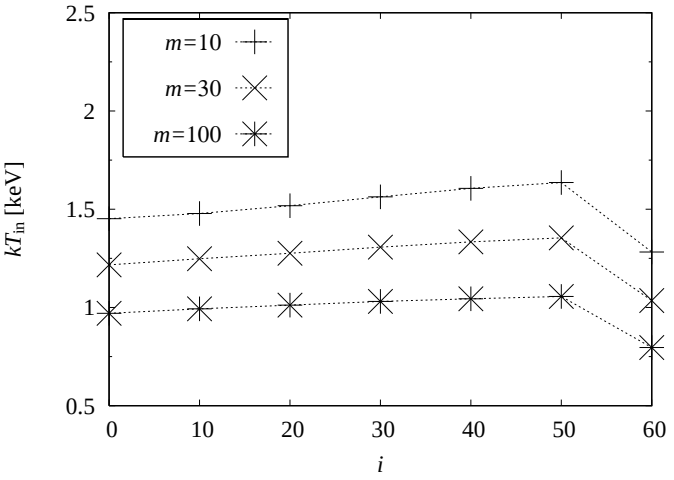

Fig. 5. Fitting results: $kT_{\rm in}$ with $m = 10$, 30, and 100 and $\dot{m} = 100$ for various i.

3.2.4. Mass Correction Factor, $m/m_{\rm x}$

Let us now examine the mass correction factor, which we define as the ratio between the real black hole mass, m, to the estimated mass by the X-ray spectral fitting, $m_{\rm x}$. Here, we adopt the assumption used in the conventional disk blackbody model, that is $r_{\rm in} = 3r_{\rm g}$.

Firstly, let us see the dependence of the correction factor on $\dot{m}$ (figure 4). Here, we fix $i = 0$ and consider three different masses: $m = 10$, 30, and 100. Interestingly, we can see a similar trend in all cases; the correction factor increases as the mass-accretion rate increases. Interestingly, we can see that the correction factor also seems to depend on the black-hole mass (see table 4). It follows a similar trend as that of $\dot{m}$; that is, a larger correction factor is needed for a larger black-hole mass, although it is less prominent for the small $\dot{m}$ case.

These findings show that correction factor (~ 2) is needed when we work with the system of high m and $\dot{m}$. Unfortunately, those are indeed two pieces of information that we intend to find. However, since we are interested in the high temperature ULXs, we suggest the correction factor of 1.2 – 1.3 and 1.3 – 1.6 for $m = 10$ and 30, respectively, depending on the mass-accretion rate.

Next, let us see the dependence of the correction factor on the inclination angle (figure 6). We found that as long as we consider inclination angles below 50°, the correction factor does not have a strong dependence on the inclination angle. Here, we show three examples for $\dot{m} = 100$: $m = 10$, 30, and $m = 100$.

To summarize, for high $\dot{m}$-case, we need a mass correction factor defined as $m/m_{\rm x}$.

Before leaving this section, it is important to note that in calculating the disk structure, and thus the spectrum, we set the inner calculation boundary at $2r_{\rm g}$. On the other hand, to derived the black hole mass we adopt $r_{\rm in} = 3r_{\rm g}$. Since the correction factor that we found here varies with m and also $\dot{m}$, we conclude that the inner radius obtained from the fitting does not represent the inner

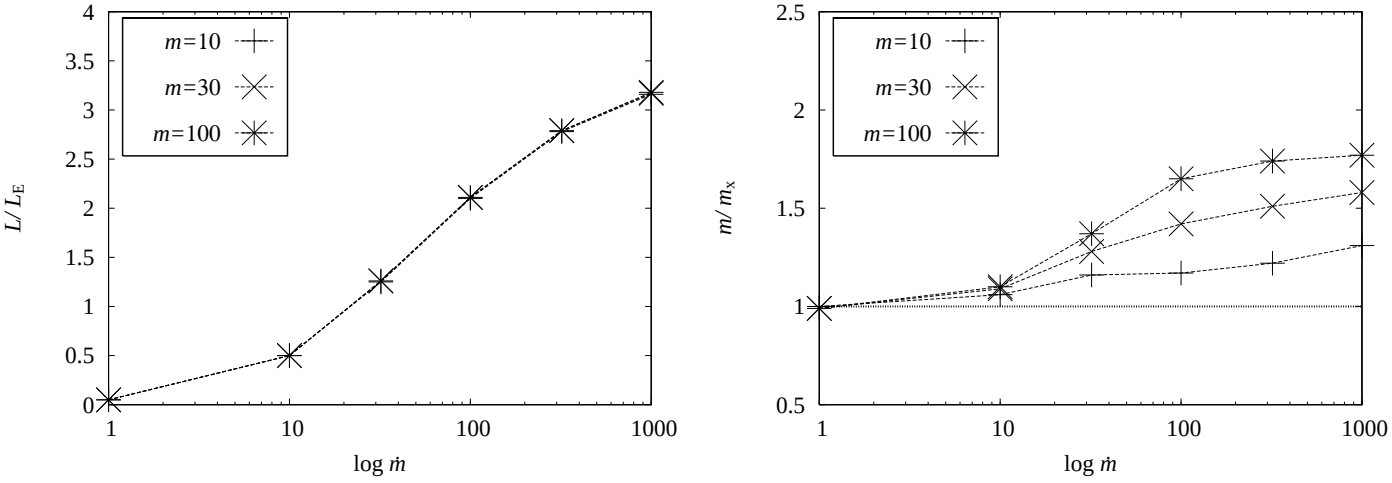

Fig. 4. Fitting results: $L/L_{\rm E}$ (left panel) with $i=0$ and $m=10,\ 30$, and the correction factor (right panel), $m/m_{\rm x}$, for various $\dot{m}$, calculated for $m=10,\ 30$, and 100 with $i=0$.

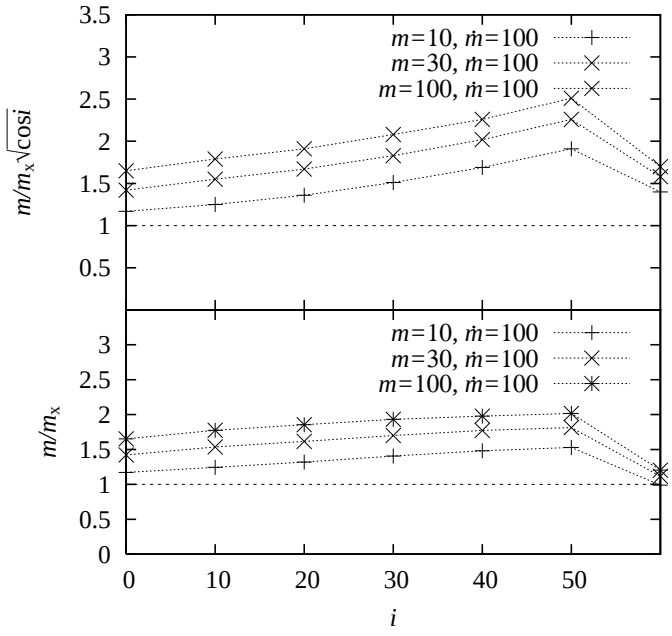

Fig. 6. Correction factor ($\equiv m/m_{\rm x}$). Top panel: for $m=10,\ 30$, and 100 and $\dot{m}=100$ for various i when i is unknown. Bottom panel: same as top panel but when i is known.

edge of the disk as was stressed in Watarai and Mineshige (2003a). They suggest that the inner radius from the fitting represents the radiation edge outside which substantial emission is produced. In fact, for super-critical accretion disks, the emission produced inside $3r_{\rm g}$ is really significant (Watarai et al. 2000).

3.3. X-ray HR Diagram

Finally, we plot our results in the so-called X-ray HR diagram, which shows the relation of X-ray luminosity, $L_{\rm x}$, with the inner temperature (in keV), $kT_{\rm in}$, obtained from the fitting (figure 7). Here, we now include the correction for $T_{\rm in}$ in the X-ray HR diagram. That is $T_{\rm in}=\kappa T_{\rm eff}/1.2$

We plot for $m=10$ (in black '+'), 30 (in black '$\times$'), and 100 (in black '$*$') and $\dot{m}=1,\ 10,\ 32,\ 100,\ 320$, and 1000, while $i=0$. This figure is similar to that of Watarai et al. (2005). However, in their paper, they only calculated for $m=10$, and then interpolated the results for higher black-hole masses. We also have included the required corrections discussed in subsection 3.1.

For low $\dot{m}$, our results follow $L\propto T_{\rm in}^4$, as expected from the sub-critical accretion (standard accretion disk) theory. For high $\dot{m}$ our results follow $L\propto T_{\rm in}^2$. We also plot some ULXs and well-known BHCs by using the references in Vierdayanti et al. (2006). For BHC whose inclination angle has been known, we included it in calculating the luminosity, while for those whose inclination angle is unknown, we assumed a face-on case. Some ULXs can very likely be explained as stellar-mass black holes with a super-critical mass accretion rate. Except for the source

Table 4. Fitting results with the extended DBB model for $\alpha=0.01$ and $i=0$. $\xi^{\rm trans}=0.353$ is assumed to derive $r_{\rm in}$ and the real $kT_{\rm in}$ is the value in the table multiplied by $\kappa^{\rm trans}$.

m	$\dot{m}$	p	$kT_{\rm in}$	$r_{\rm in}/r_{\rm g}$	$m/m_{\rm x}$	$L/L_{\rm E}$
10	32	0.605	1.27	2.55	1.16	1.25
10	100	0.559	1.45	2.52	1.17	2.10
10	320	0.518	1.59	2.41	1.22	2.78
10	1000	0.498	1.70	2.25	1.31	3.16
30	32	0.583	1.02	2.30	1.28	1.26
30	100	0.535	1.22	2.08	1.42	2.11
30	320	0.500	1.34	1.96	1.51	2.79
30	1000	0.484	1.42	1.87	1.58	3.17
100	32	0.563	0.78	2.16	1.37	1.26
100	100	0.511	0.97	1.79	1.65	2.11
100	320	0.484	1.07	1.70	1.74	2.79
100	1000	0.474	1.11	1.67	1.77	3.18

Table 5. Same as table 4 but here we fixed $\dot{m} = 100$ while varying the inclination angle, i.

m	i	p	$kT_{\rm in}$	$r_{\rm in}/r_{\rm g}$	$m/m_{\rm x}$	$L/L_{\rm E}$
10	0	0.559	1.45	2.52	1.17	2.10
10	10	0.553	1.48	2.37	1.24	1.97
10	20	0.552	1.52	2.24	1.32	1.86
10	30	0.553	1.56	2.10	1.40	1.70
10	40	0.558	1.60	1.99	1.48	1.50
10	50	0.566	1.64	1.93	1.53	1.28
10	60	0.585	1.28	2.99	0.99	0.90
30	0	0.535	1.22	2.08	1.42	2.11
30	10	0.528	1.25	1.92	1.54	1.97
30	20	0.529	1.28	1.83	1.62	1.86
30	30	0.532	1.31	1.74	1.70	1.70
30	40	0.538	1.33	1.67	1.77	1.51
30	50	0.546	1.35	1.63	1.81	1.28
30	60	0.562	1.04	2.65	1.12	0.90
100	0	0.511	0.97	1.79	1.65	2.11
100	10	0.506	0.99	1.66	1.78	1.98
100	20	0.508	1.01	1.59	1.85	1.86
100	30	0.512	1.03	1.53	1.93	1.70
100	40	0.520	1.04	1.49	1.98	1.51
100	50	0.528	1.06	1.47	2.02	1.28
100	60	0.541	0.80	2.46	1.20	0.90

IC 342 S1, Vierdayanti et al. (2006) fitted the other ULX data with the extended DBB model. The data of IC 342 S1 are taken from Mizuno et al. (2001), in which they fitted the ASCA data with the multicolor disk blackbody (DBB) model.

The red dotted lines shows the masses and η ($\equiv L/L_{\rm E}$) which were calculated from the standard disk relations [see Makishima et al. 2000 equation (9) and (11)]. We also plot the fitting results from Shakura and Sunyaev analytical solutions (see section 3.1) in red '$\otimes$'mark. We can thus safely conclude that the black holes in ULXs, which Vierdayanti et al. (2006) analyzed, are stellar-mass black holes with mass $< 100 M_{\odot}$.

4. Discussion

In this section we would like to discuss some important issues that are related to our present study. The first and the most important issue is the dependence of the fitting results on the fitting energy range. The next two issues are the spectral hardening factor, which remains an open question for the case of super-critical accretion, and outflow of material from the disk. Another interesting issue is the formation scenario of ULX in terms of binary star evolution. Supposing some ULXs are highly accreting stellar-mass black holes, it is very natural to think that those ULXs are binary systems and the disk material is supplied by their companions. In the last part of this section, we comment on other plausible black hole mass estimation methods for ULXs.

4.1. Dependence on the Fitting Energy Range

It is very important to note that the fitting results sensitively depend on the fitting energy range. In our present study, we fixed the fitting energy range to be 0.3 – 10 keV which is normally used in the study of BHBs as well as ULXs. Therefore, it is interesting to know how the fitting results will change if we choose a different fitting energy range. It will be necessary at some later time when the observations could provide us with data of a wider energy range. We extend our results to the higher energy part of the spectrum, so that we can also predict some features that had not been made available much by observations. On the other hand, we do not consider the lower energy part, lower than 0.3 keV, since there remains some difficulties in the analysis of this energy part due to the effect of the interstellar medium.

We, therefore, performed the same procedure as what we explain in section 3 for a larger fitting energy range, 0.3 – 30 keV. We summarize the fitting results in table 6. We obtained higher $T_{\rm in}$ and lower $r_{\rm in}$; as a consequence we have larger mass correction factor, ranging from 1.4 – 1.9 ($m = 10$), 1.4 – 2.0 ($m = 30$), and 1.4 – 2.1 ($m = 100$). To conclude our discussion in this subsection, we need a mass correction, $m/m_{\rm x} \sim 2$ at most, for fitting with a wider energy range, which can be use as a reference when the observational data are available.

4.2. Spectral Hardening

The spectral hardening factor plays an important role in estimations of the black-hole mass, particularly when it is based on the X-ray spectral fitting. As mentioned in section 3, the spectral hardening factor is usually set to be 1.7 for the standard accretion disk. This value was obtained from a numerical calculation of the vertical structure and the radiative transfer of an accretion disk around a Schwarzschild black hole by Shimura and Takahara (1995), in which a geometrically thin disk assumption is used. Their results imply that the X-ray spectrum of a standard disk is affected by Comptonization, and the local flux can be approximated by a diluted blackbody flux (see subsection 2.2), with $\kappa \sim 1.7$ (see also Czerny & Elvis 1987; Ross et al. 1992).

We are aware that the bound-free opacity may still play an important role, and that it is important to address this issue properly. In our present study, however, we did not include the effect of bound-free opacity, and we simply mimicked the deviation from the blackbody spectra by a diluted blackbody approximation without considering the details of the physical mechanism that may produce it. In fact, we also think that it is even possible that the spectrum at high-energy part may experience softening as well (Ohsuga et al. 2003; Suleimanov & Poutanen 2006). In order to address these issues properly, we need to work with radiative transfer, which is beyond the scope of our present study. Regarding the effect of the bound-free opacity on the spectral shape, it will be necessary for the readers to consult other papers (e.g., Suleimanov & Poutanen 2006). Meanwhile, we continue our discussion

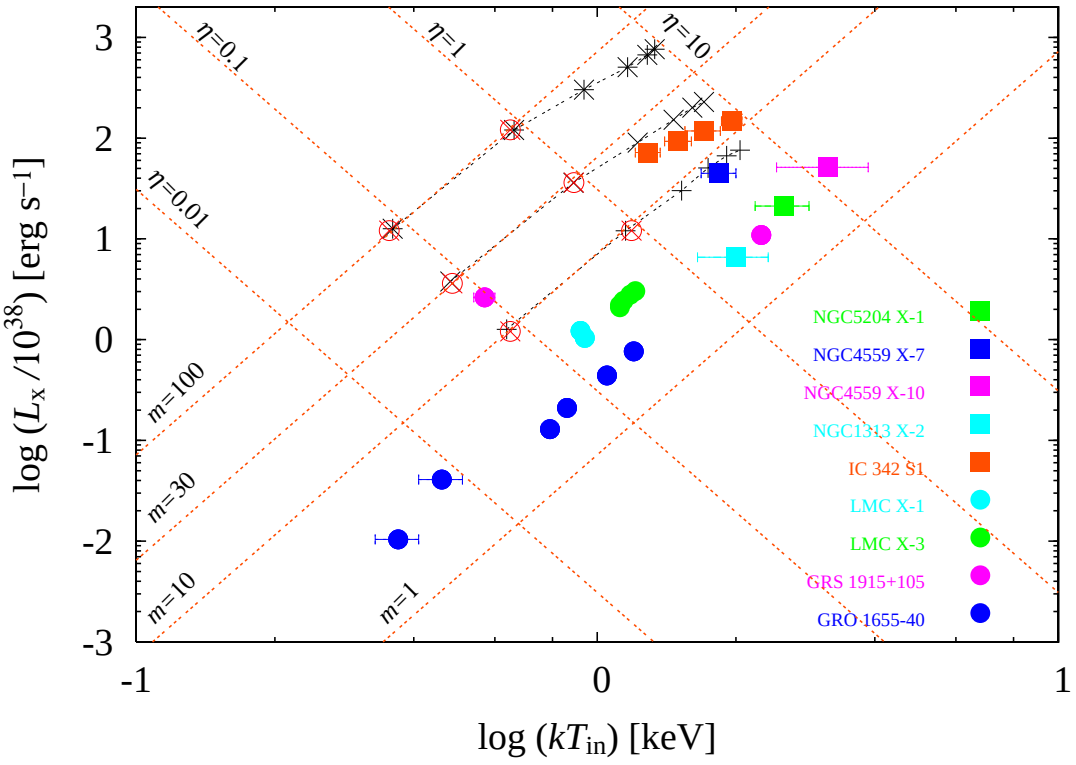

Fig. 7. Luminosity vs. temperature diagram for various m ($m = 10$ in black '+', $m = 30$ in black '×', and $m = 100$ in black '∗') and $\dot{m} = 1$, 10, 32, 100, 320, and 1000 (increasing with luminosity and kT_{in}), while $i = 0$. Several ULXs (NGC 5204 X-1, NGC 4559 X-7, NGC 4559 X-10, NGC 1313 X-1, and IC 342 Source 1) and some well-known black hole candidates (LMC X-1, LMC X-3, GRO 1655-40, and GRS 1915+105) are included in the diagram (reference:Vierdayanti et al. 2006, Watarai et al. 2005). Red '⊗'symbols are calculated from analytical solution of standard disk and red lines are calculated from standard disk relations (see text, section 3.3).

in the context of the diluted blackbody approximation in which spectral hardening factor plays a key role.

Merloni et al. (2000) analyzed the spectral hardening factor used to correct the fitting results of the DBB model. They use a self-consistent model for the radiative transfer and the vertical temperature structure in a standard disk to simulate the observed disk spectra. In addition, they also take into account the gravitational redshift and transverse Doppler effects. They fitted this model to the DBB model, and found that the spectral hardening factor is not constant; the spectral hardening factor becomes higher when the accretion rate and/or coronal activity is high. The range of the varying hardening factor is within $1.7 < \kappa < 3$. Davis et al. (2006) also show significant spectral hardening when a disk becomes effectively optically thin.

In terms of super-critical accretion model, Kawaguchi (2003) showed that spectral hardening by electron scattering is quite α sensitive, since $\tau_{es}/\tau_{abs} \propto \alpha^{1/8}$. Therefore, an increase of α results in an increase of the color temperature, and thus we get more spectral hardening. Note that all the spectral calculations mentioned above assume hydrostatic disk layers.

In the present study, we set the spectral hardening factor to be, $\kappa = 1.7$, the widely used value for the case of sub-critical (standard) accretion due to the uncertainty of the κ in the case of super-critical accretion. The choice of other value of κ would certainly affect the spectrum shape, for instance, choosing $\kappa > 1.7$ will cause the spectrum to be harder in the high energy band and the slope in the lower energy band would also be changed. $\kappa \sim 3$ was suggested for high luminosity disks (Watarai & Mineshige 2003b). Since the derived black-hole mass from the fitting depends on κ as $M \propto \kappa^2$, a mass underestimation/overestimation is possible due to the choice of κ.

To summarize, there remain uncertainties in the spectral hardening factor of super-critical accretion flow. This will, in turn, introduce another source of uncertainty in our present mass estimation. A more complete description of spectral properties of super-critical accretion is awaited.

4.3. Outflow of Material

Through a 2-dimensional radiation-hydrodynamic simulation Ohsuga et al. (2005) found high-speed outflow (with 10–20 % of speed of light) from the center of super-critical flow with a rate of $\sim L_E/c^2$. This nearly relativistic motion will affect the photon spectra, whose effect depends on the inclination angle of the system (Heinzeller et al. 2006).

In fact, Heinzeller et al. (2006) found that the aver-

age photon energy due to a shift of the frequency of the escaping photons by the relativistic Doppler effect in a face-on case (small inclination angle) is of a factor of 1.18 higher than that of the edge-on case (large inclination angle). They also reported that the main features of the thermal component of the spectrum of super-critical accretion flow are consistent with the slim disk, while there remain unresolved features in the high-energy part. This kind of simulation is very important to address the effect of the outflow in the observed spectrum. However, an adequate calculation resolution has not been available at the moment.

In the meantime, as a qualitative study, we compare two different cases. The first case is a disk with advection without outflow (our case), and the second case is the disk with outflow without advection, which was first considered by Shakura and Sunyaev (1973), as also discussed in Poutanen et al. (2007). In addition to the fact that both cases result in similar temperature profiles, $T_{\rm eff} \propto r^{-1/2}$ (flatter temperature distribution than that of the standard disk), we found another interesting fact.

Both cases have a characteristic radius. In the advection case, it is called the trapping radius, $r_{\rm tr}$, inside of which the diffusion timescale is longer than the accretion timescale (and thus the photon trapping becomes important). In the outflow case, it is called the spherization radius, $r_{\rm sp}$, at which the disk luminosity is close to the Eddington luminosity (Lipunova 1999). Interestingly, those two radii are comparable or, to be more precise, the spherization radius is twice as small as the trapping radius: $r_{\rm tr} \sim \dot{m} r_{\rm g}/2$ while $r_{\rm sp} \sim \dot{m} r_{\rm g}/4$, if we set $H/r \sim 1$ for the advection case. This means that the advection effect becomes effective even before the outflow needs to set in to remove any excess of the gravitational energy caused by high mass-accretion rate inflow of the disk materials.

Although it is necessary to address this issue more properly, especially when both advection and outflow occur simultaneously (see also Poutanen et al. 2007), we did not include the effect of the outflow in our present study, while assuming that the advection works effectively.

4.4. On Black-Hole Binary Evolution

The work in the disk model is indeed synchronized by the work in the field of black-hole evolution in binary systems. We point out some studies on black-hole binary evolution in this section.

King et al. (2001), for example, proposed a mild X-ray beaming model for ULXs. Their model suggest that ULXs may represent the phase of thermal-timescale mass transfer that occurs in high-mass X-ray binaries. This phase is short-lived, but is extremely common in the evolution of X-ray binaries. The short lifetimes of high-mass X-ray binaries could explain the association of ULXs with the star-formation region. Moreover, in the context of a binary system, their model does not require IMBH to explain the nature of ULXs.

Rappaport et al. (2005) suggest that the luminosity of ULXs can be explained by a stellar-mass black hole in a binary with a moderate mass companion. They follow the evolution of the binary before the black hole is formed until it emits the X-ray by the accretion process onto the black hole. They found that luminosities of the order of ULX luminosities can be produced if the Eddington limit is allowed to be exceeded by about a factor of ten. Interestingly, this clearly supports super-critical accretion flow onto a black hole as a possible mechanism for ULXs.

4.5. Other Black Hole Mass Estimation Methods

Despite being very useful, some uncertainties remain concerning mass estimation through the X-ray spectral fitting as a result of its attachment on some assumptions. Therefore, mass estimation from other independent methods are eagerly awaited to settle the dispute over the black-hole mass of the ULXs. It also remains possible that ULXs cannot be explained by a single theoretical model.

Despite being widely used when the dynamical mass estimation method cannot be applied, the X-ray spectral fitting is not the only method to estimate the black-hole mass. Indeed, other independent mass estimation is demanded to settle the dispute over the black hole mass of the ULXs. One of the other independent mass estimations is by double peak quasi-periodic oscillation (QPOs) in a 3:2 ratio to be discovered in the time variability of ULXs (Abramowicz et al. 2004). These QPO frequencies scale inversely with the mass of the source, which was first shown for microquasars by McClintock and Remillard (2003), and more recently for low-mass Seyfert galaxies by Lachowicz et al. (2006). For ULXs, in general, it has not been detected yet. Recently, Strohmayer et al. (2007) reported possible double peak QPOs in NGC 5408 X-1 which happened to have 4:3 ratio. Unfortunately, the scaling law of the upper frequency QPO and the mass is not obvious for QPOs other than that with a 3:2 ratio.

Other scaling laws are found in X-ray binaries and active galactic nuclei (AGNs). It was found that the ratio of the radio to X-ray emission depends strongly on the black hole mass (Falcke et al. 2004). If ULXs are in the same family with our Galactic X-ray binaries in the very high state, it is expected that they could also be radio transients. In this regard, Körding et al. (2004) conducted a radio-monitoring study of ULXs in nearby galaxies with the VLA. Körding et al. (2005) found that generally ULXs do not emit steady-state radio emission above radio powers of 1.5×10^{17} W/Hz, and thus radio loud ULXs is still awaited to be found.

Pooley and Rappaport (2005) suggest that X-ray and optical eclipses can be used to distinguish the two possible black hole masses. ULXs with stellar-mass black holes should exhibit at least twice as many eclipses as would IMBH systems. They proposed X-ray monitoring campaigns for a few days to detect eclipses. In the optical range, monitoring ~ 10 ULXs twice a night each for a couple of months by using ground-based telescope should also work.

Meanwhile, we can merely rely on X-ray spectral fitting which was found to be quite a reliable method in the case of Galactic black-hole binaries.

Table 6. Same as table 4 but the energy range for fitting is 0.3 – 30 keV.

m	$\dot{m}$	p	$kT_{\rm in}$	$r_{\rm in}/r_{\rm g}$	$m/m_{\rm x}$	$L/L_{\rm E}$
10	32	0.58	1.39	2.12	1.39	1.25
10	100	0.53	1.79	1.66	1.78	2.10
10	320	0.50	1.96	1.59	1.86	2.78
10	1000	0.48	2.04	1.57	1.88	3.16
30	32	0.57	1.07	2.08	1.42	1.26
30	100	0.51	1.41	1.56	1.90	2.11
30	320	0.48	1.54	1.49	1.99	2.79
30	1000	0.47	1.60	1.48	2.00	3.17
100	32	0.55	0.80	2.06	1.40	1.26
100	100	0.49	1.07	1.48	2.00	2.11
100	320	0.47	1.17	1.41	2.09	2.79
100	1000	0.46	1.21	1.41	2.09	3.18

5. Conclusion

We have analyzed the assumption $r_{\rm in} = 3r_{\rm g}$ for black hole mass estimation for the case of super-critical accretion disk.

We fitted the slim disk spectra for various parameter combinations (m, $\dot{m}$, and i), with the extended disk blackbody model. We fixed $\alpha = 0.01$ in the disk structure calculation, and chose $\kappa = 1.7$ for the spectrum calculation. To estimate the black hole mass, we adopt $\xi^{\rm trans} = 0.353$.

As expected from a theoretical point of view, we obtained p-values that deviate from 0.75, the value expected for the standard disk model. Moreover, we found that by adopting, the assumption $r_{\rm in} = 3r_{\rm g}$ for a slim disk, the estimated black hole mass should be corrected. The correction factors are 1.2 – 1.3 and 1.3 – 1.6 for $m = 10$ and $m = 30$, respectively. Since the corrections are small, we can safely conclude that the black holes in ULXs which Vierdayanti et al. (2006) analyzed are stellar-mass black holes with mass $< 100 M_\odot$.

We gratefully thank the anonymous referees for their useful comments and suggestions concerning the first manuscript of this paper. This work was supported in part by the Grants-in-Aid of the Ministry of Education, Science, Culture, and Sport (14079205, 16340057 S.M.; 16004706 K.W.), by the Grant-in-Aid for the 21st Century COE "Center for Diversity and Universality in Physics" from the Ministry of Education, Culture, Sports, Science and Technology (MEXT) of Japan. One of the authors, K.V., gratefully thank the MEXT scholarship.

References

Abramowicz, M. A., Czerny, B., Lasota, J. P., & Szuszkiewicz, E. 1988, ApJ, 332, 646
Abramowicz, M. A., Kato, S., & Matsumoto, R. 1989, PASJ, 41, 1215
Abramowicz, M. A., Kluźniak, W., McClintock, J. E., & Remillard, R. A. 2004, ApJ, 609, L63
Colbert, E. J. M., & Mushotzky, R. F. 1999, ApJ, 519, 89
Cropper, M., Soria, R., Mushotzky, R. F., Wu, K., Markwardt, C., B., & Pakull, M. 2004, MNRAS, 349, 39
Cunningham, C. T. 1975, ApJ, 202, 788
Czerny, B., & Elvis, M. 1987, ApJ, 321, 305
Davis, S. W., Done, C., & Blaes, O. M. 2006, ApJ, 647, 525
Dotani, T, et al. 1997, ApJL, 485, 87
Ebisawa, K. 1999, ASPC, 161, 39
Ebisawa, K., Mitsuda, K., & Hanawa, T. 1991, ApJ, 367, 213
Ebisawa, K., Życki, P., Kubota, A., Mizuno, T., & Watarai, K. 2003, ApJ, 597, 780
Falcke, H., Körding, E., & Markoff, S. 2004, A&A, 414, 895
Fukue, J. 2000, PASJ, 52, 829
Fukue, J., & Yokoyama, T. 1988, PASJ, 40, 15
Gierliński, M., Zdziarski, A. A., Poutanen, J., Coppi, P. S., Ebisawa, K., & Johnson, W. N. 1999, MNRAS, 309, 496
Heinzeller, D., Mineshige, S., & Ohsuga, K., 2006, MNRAS, 372, 1208
Hoshi, R. 1977, PThPh., 58, 1191
Jaroszyński, M., Abramowicz, M. A., & Paczynski, B. 1980, AcA, 30, 1
Kato, S., Fukue, J., Mineshige, S. 2008, Black-Hole Accretion Disks (Kyoto: Kyoto University Press)
Kawaguchi, T. 2003, ApJ, 593, 69
King, A. R., Davies, M. B., Ward, M. J., Fabbiano, G., & Elvis, M. 2001, ApJ, 552, L109
Körding, E., Colbert, E., & Falcke, H. 2004, PThPS, 155, 365
Körding, E., Colbert, E., & Falcke, H. 2005, A&A, 436, 427
Kubota, A. 2001, Ph.D. thesis, Univ. Tokyo
Kubota, A., Tanaka, Y., Makishima, K., Ueda, Y., Dotani, T., Inoue, H., & Yamaoka, K. 1998, PASJ, 50, 667
Lachowicz, P., Czerny, B., & Abramowicz, M. A. 2006, astro-ph/0607594
Lipunova, G. V. 1999, AstL, 25, 508
Luminet, J. P. 1979, A&A, 75, 228
Madhusudhan, N., Justham, S., Nelson, L., Paxton, B., Pfahl, E., Podsiadlowski, Ph., & Rappaport, S. 2006, ApJ, 640, 918
Makishima, K., et al. 1986, ApJ, 308, 635
Makishima, K., et al. 2000, ApJ, 535, 632
Matsumoto, R., Kato, S., Fukue, J., & Okazaki, A. T. 1984, PASJ, 36, 71
McClintock, J. E., & Remillard, R. A. 2003, astro-ph/0306213
Merloni, A., Fabian, A. C., & Ross, R. R. 2000, MNRAS, 313, 193
Miller, J. M., Fabbiano, G., Miller, M. C., & Fabian, A. C. 2003, ApJ, 585, L37
Miller, J. M., Fabian, A. C., & Miller, M. C. 2004, ApJ, 614, L117
Mineshige, S., Hirano, A., Kitamoto, S., Yamada, T. T., & Fukue, J. 1994, ApJ, 426, 308
Mizuno, T., Kubota, A., & Makishima, K. 2001, ApJ, 554, 1282
Ohsuga, K., Mineshige, S., & Watarai, K. 2003, ApJ, 596, 429
Ohsuga, K., Mori, M., Nakamoto, T. & Mineshige, S. 2005, ApJ, 628, 368
Okajima, T., Ebisawa, K., & Kawaguchi, T. 2006, ApJL, 652, 105
Paczynski, B. & Wiita, P. J. 1980, A&A, 88, 23
Pooley, D. & Rappaport, S. 2005, ApJ, 634, L85
Poutanen, J., Lipunova, G., Fabrika, S., Butkevich, A.G., & Abolmasov, P. 2007, MNRAS, 377, 1187
Rappaport, S. A., Podsiadlowski, Ph., & Pfahl, E. 2005, MNRAS, 356, 401

Roberts, T. P., Warwick, R. S., Ward, M. J., Goad, M. R., & Jenkins, L. P. 2005, MNRAS, 357, 1363
Ross, R. R., Fabian, A. C., & Mineshige, S. 1992, MNRAS, 258, 189
Shakura, N. I., & Sunyaev, R. A. 1973, A&A, 24, 337
Shimura, T., & Takahara, F. 1995, ApJ, 445, 780
Strohmayer, T. E., Mushotzsky, R. F., Winter, L., Soria, R., Uttley, P., & Cropper, M. 2007, ApJ, 660, 580
Suleimanov, V., & Poutanen, J. 2006, MNRAS, 369, 2036
Szuszkiewicz, E., Malkan, M. A., & Abramowicz, M. A. 1996, ApJ, 458, 474
Tanaka, Y., & Shibazaki, N. 1996, ApJ, 34, 607
Tsunoda, N., Kubota, A., Namiki, M., Sugiho, M., Kawabata, K., & Makishima, K. 2006, PASJ, 58, 1081
Vierdayanti, K., Mineshige, S., Ebisawa, K. & Kawaguchi, T. 2006, PASJ, 58, 915
Wang, J. M., & Zhou, Y. Y. 1999, ApJ, 516, 420
Watarai, K., & Fukue, J. 1999, PASJ, 51, 725
Watarai, K., Fukue, J., Takeuchi, M., & Mineshige, S. 2000, PASJ, 52, 133
Watarai, K. & Mineshige, S. 2003b, ApJ, 596, 421
Watarai, K. & Mineshige, S. 2003a, PASJ, 55, 959
Watarai, K., Mizuno, T., & Mineshige, S. 2001, ApJ, 549, L77
Watarai, K., Ohsuga, K., Takahashi, R., & Fukue, J. 2005, PASJ, 57, 513